Design Limitations of Highly Parallel Free-Space Optical Interconnects Based On Arrays of Vertical-Cavity Surface Emitting Laser Diodes, Microlenses, and Photodetectors

Suning Tang, Ray T. Chen
Dave Gerold, Maggie M. Li, Chunhe Zhao, Srikanth Natarajan and Jielun Lin
Microelectronics Research Center
Department of Electrical and Computer Engineering
University of Texas, Austin, Texas 78712-1084
Tel: 512-4717035

Abstract

The packing density of a highly parallel free-space multi-stage optical interconnect network involving arrays of vertical cavity surface-emitting lasers (VCSELs), microlenses and photodetectors is analyzed for the first time, based on a crosstalk model involving the diffraction-induced crosstalk among pixels. Variations of channel packing density, interconnection distance and optical transmission efficiency are evaluated to provide optimum design parameters for the arrays of VCSELs, microlenses and photodetectors. It is shown that it is pivotal to optimize the photodetector diameter in such an optical interconnect network. Photodetector array misalignment effects on system performance are further investigated, providing both transverse and longitudinal alignment tolerance. Several experiments are also conducted to verify the theory developed herein.

1. Introduction

Advancements in micro-fabrication have permitted electronic devices to be packed ever more densely, resulting in a consequent increase in the number of signal paths needed for device interconnects. This, combined with constantly increasing demand for signal speed, has resulted in problems of clock skew and bandwidth limitation of electrical interconnects. Free-space optical interconnects are of increasing importance as an attractive replacement for electrical interconnects in high performance digital computers[1-4]. Very recently, a new type of free-space optical interconnect, based on a microlens array, a surface-emitting laser diode array and a photodetector array, was proposed along with preliminary demonstrations[5-7]. A number of advantages are associated with such an optical interconnect (OI) architecture. These include high efficiency, massive parallelism, wide bandwidth and high speed.

As one of the key parameters of an OI network, the packing density (number of pixels/cm^2) has been investigated for various OI networks[8-10]. Analytic techniques used include an application of Gabor's theory in a free-space interconnect[11], a multiple-scattering model in volume holographic interconnections[12], and a crosstalk model relating the cross-coupling among channel waveguides[13,14]. Ray-tracing and Gaussian beam estimations were used to study the device performance in two previously reported highly parallel free-space optical interconnect networks based on arrays of vertical cavity surface-emitting lasers (VCSELs) and microlenses[5,6]. In both estimations, optical beam spreading due to the finite aperture of the laser cavity and lens aperture was not considered. As a result, the system performance, including channel packing density, interconnect length, optical transmission efficiency and signal-to-noise (S/N) ratio, cannot be accurately determined. In fact, it has been found that diffraction is the dominant effect and thus imposes a major limitation on the interconnectivities of such free-space optical interconnect networks.

0-8194-1448-4/94/$6.00

In this paper, diffraction induced cross-coupling among pixels is included in the crosstalk model. This model is developed to study packing density of the highly parallel free-space multi-stage optical interconnect network shown in Fig. 1, where arrays of VCSELs, microlenses and photodetectors are presented. Based on the crosstalk model, variations of packing density, interconnection length and optical transmission efficiency are investigated. Misalignment effects on system performance are also studied and the resultant effects on both transverse and longitudinal alignment tolerance of the photodetector array are presented. To verify the theory presented, some experiments were conducted and the results showed good agreement with the theory. Optimum design criteria for the radii of laser output window, microlens and photodetector are further delineated for the first time.

2. Basic Relations

The schematic diagram representing the system under consideration is shown in Fig. 1, which presents an array of VCSELs with an output window of radius a, followed by an array of microlenses with lens radius ω_0 and focal length f. An array of photodetectors with a detector radius of a_d are located at the receiving plane as shown in Fig. 1. The detector separation is $2\rho_s$. The distance between the laser diode array and the microlens array is equal to the focal length. The separation between the microlens array and the photodetector array is defined as the interconnection distance. This is a space-invariant linear operation system[11]. Based on Gabor's theory of information, circular symmetry of the optical elements (laser diodes, lenses and detectors) represents the highest degree of symmetry and is preferred for the best interconnect fidelity[11]. We thus select circular symmetry in the following discussion. The arranging lattice of the two-dimensional array (see Fig. 1) is a square-packed pattern, which has been used by previous researchers[3,5,6].

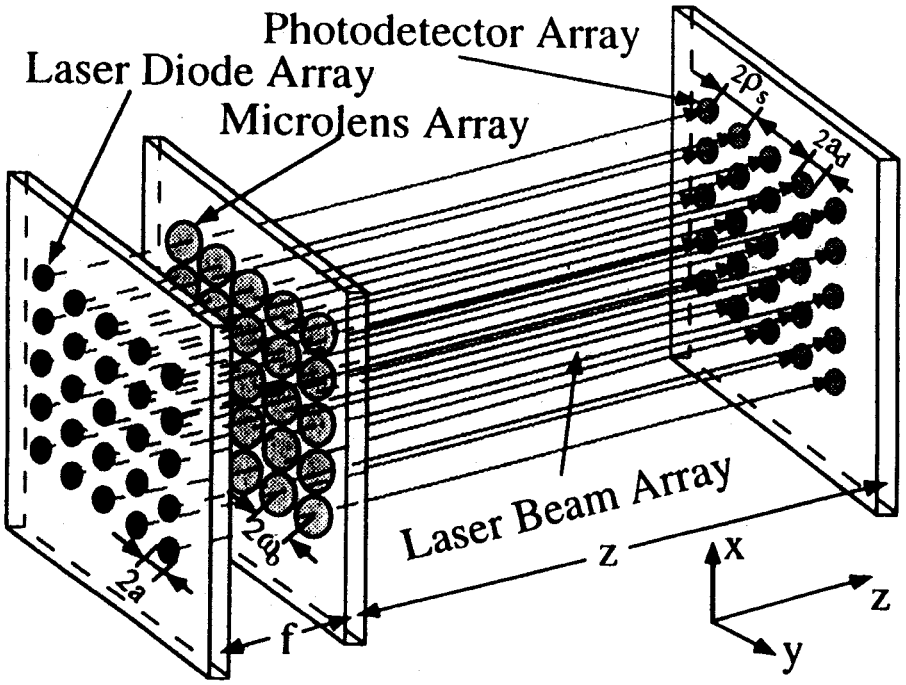

Figure 1: A schematic diagram of a highly parallel free-space optical interconnect based on arrays of surface-emitting laser diodes, microlenses and photodetectors.

The optical wave emitted from the vertical cavity surface-emitting laser diode in this case is a plane wave diffracted by an output window with a finite aperture[15,16]. Accepting the validity of the Fraunhofer approximation[6,17], i.e., $\frac{a^2}{2\lambda} << f$, we derive the normalized amplitude of the electrical field distribution $E(\omega)$ which is the Fourier-Bessel transform of $E(r)$ at the microlens array plane, evaluated at spatial frequency $\frac{\omega}{\lambda f}$. The result is given by

$$E(\omega) = \boldsymbol{B}\{E(r)\} = \frac{J_1(ka\omega/f)}{(ka\omega/f)} \quad \text{and,} \qquad (1)$$

$$E(r) = \text{circ}(\frac{r}{a}) = \begin{cases} 1 & (r \le a) \\ 0 & (\text{otherwise}) \end{cases} \qquad (2)$$

where $\boldsymbol{B}$ stands for the Fourier-Bessel transformation and $\text{circ}(\frac{r}{a})$ accounts for the finite aperture of the laser output window with radius of a. J_1 is the first order Bessel function of the first kind while r and ω are, respectively, the radii in polar coordinates in the plane of the laser output window and the plane of the microlens(see Fig. 1). The wave vector in free-space is $k = 2\pi/\lambda$ where λ is optical operating wavelength. Denoting $P(\omega_o)$ as the fraction of the total normalized power contained within the circular aperture of a lens with radius of ω_o (see Fig. 1), we have,

$$P(\omega_o) = 2\pi \int_0^{\omega_o} |E(\omega)|^2 \, \omega d\omega = 1 - [J_0(ka\omega_o/f)]^2 - [J_1(ka\omega_o/f)]^2. \qquad (3)$$

where J_0 is the fundamental order Bessel function of the first kind. The resultant figure, representing the relationship between the laser power transmitted through the microlens and the radius of microlens, is shown in Fig. 2.

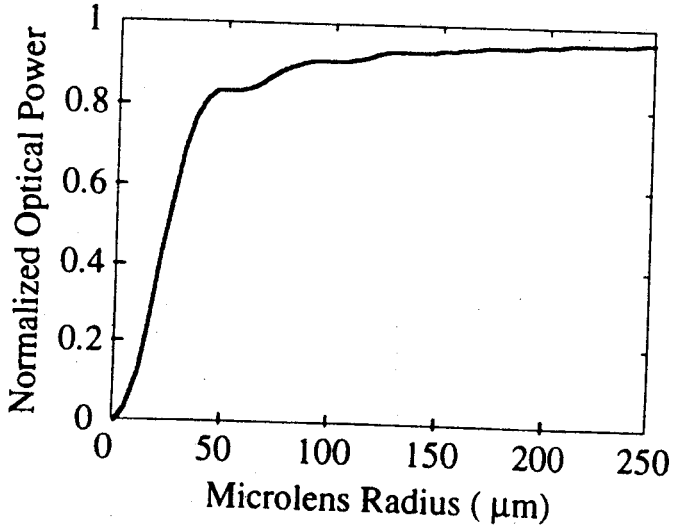

Figure 2: Calculated optical signal transmitted through a microlens. $\lambda = 0.85$ μm, $a = 5$ μm, $f = 500$ μm, and $\omega_o = 100$ μm were assumed.

In the OI system shown in Fig. 1, a fraction of the uncollected energy $(1 - P(\omega_o))$ is transmitted to other detectors through neighboring lenses. The total power of the crosstalk noise collected by each detector may be written as

$$P_{n1} = P_{n1}' + P_{n1}'' = 4\{ \int_{\omega_o}^{3\omega_o} \int_{\theta_1}^{\theta_2} |E(\omega)|^2 \, \omega d\omega d\theta + \int_{\omega_1}^{(\omega_1+2\omega_o)} \int_{\theta_3}^{\theta_4} |E(\omega)|^2 \, \omega d\omega d\theta \} \qquad (4)$$

where P_{n1}' and P_{n1}'' stand for the diffraction noises from nearest lasers and second nearest lasers collected by a detector, and $\omega_1=(2\sqrt{2}-1)\omega_o$. $\theta_2 - \theta_1$ and $\theta_4 - \theta_3$ are, respectively, the angles covered by the nearest lens and second nearest lens in reference to the origin of the polar coordinates, which coincides with the center of the microlens being considered (see Fig. 3).

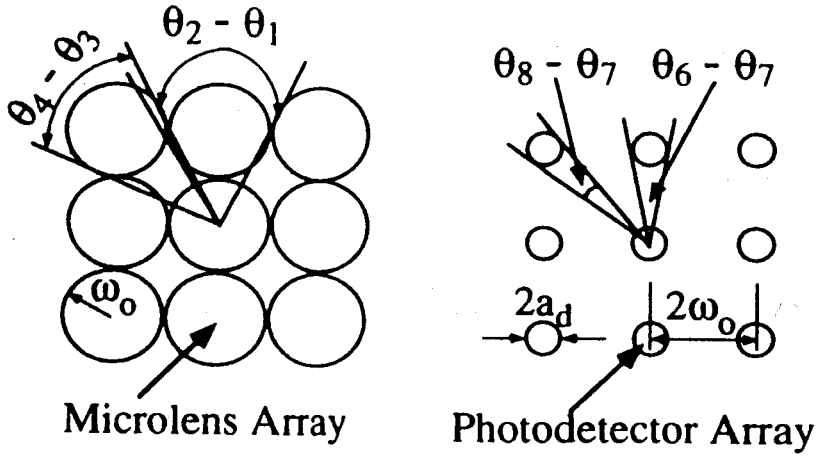

Figure 3: A front view of a portion of microlens array and photodetector array.

To determine the signal-to-noise ratio and thus the packing density, the diffraction of the lens employed has to be considered as well. Because the surface-emitting laser diode is placed at the front focal point of the lens, the output electric field from a lens can be described as a quasi-plane wave with a finite aperture of ω_o[17], i.e.,

$$E(\omega) = E(\omega) \, \mathrm{circ}\left(\frac{\omega}{\omega_o}\right), \qquad (5)$$

where the electrical field $E(\omega)$ is given by Eq. (1) and the circle function accounts for the finite lens aperture of radius ω_o. To find the distribution $E(\rho)$ of the field amplitude across the plane of the photodetector array, the Huygens-Fresnel principle[17] is applied. This gives

$$E(\rho) = \iint \frac{\exp(jkl)}{j\lambda l} \cos(\mathbf{n},l) E(\omega) d\omega d\theta \qquad (6)$$

where $l = (z^2 + \rho^2)^{0.5}$, z is the interconnection distance, and ρ is the radius in polar coordinates at the photodetector plane. $\mathbf{n}$ is the normal vector to the microlens plane. The optical signal collected by a detector with radius a_d is given as

$$P_s(a_d) = 2\pi \int_0^{a_d} |E(\rho)|^2 \rho d\rho \ . \qquad (7)$$

The relationship between the signal received by a detector and detector radius is shown in Fig. 4, based on Eq. (7). It is clear from this figure that it is not necessary to have very large photodetector radius to achieve high optical transmission efficiency. The transmission efficiency can be as high as 80% with photodetector radius of only 20 μm. Note that the optical reflection of microlenses is not considered in Eq. (7), as well as In Fig. 4.

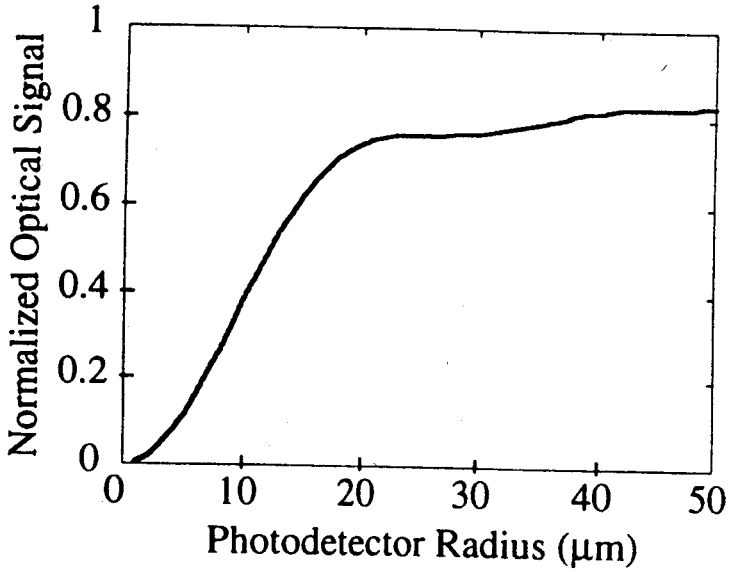

Figure 4: Calculated optical signal received by a photodetector. $\lambda = 0.85$ μm, $a = 5$ μm, $f = 500$ μm, $z = 5000$ μm and $\omega_o = 100$ μm were assumed.

The total power of the crosstalk noise P_{n2} due to lens diffraction and collected by each detector placed a distance z from the lens array plane is derived as

$$P_{n2} = P_{n2}' + P_{n2}'' = 4\{ \int_{2\rho_s - a_d}^{2\rho_s + a_d} \int_{\theta_6}^{\theta_5} |E(\rho)|^2 \rho d\rho d\theta + \int_{2\rho_s' - a_d}^{2\rho_s' + a_d} \int_{\theta_8}^{\theta_7} |E(\rho)|^2 \rho d\rho d\theta \}, \qquad (8)$$

where P_{n2}' and P_{n2}'' stand for diffraction noises from the nearest lenses and the second nearest lenses. Here, $\theta_6 - \theta_5$ and $\theta_8 - \theta_7$ (shown in Fig. 3) are the angles covered by the detector in reference to the center of the nearest and the second nearest detectors in the detector plane, $\rho_s' = \sqrt{2}\rho_s$ and $2\rho_s$ are the minimum detector-to-detector separations satisfying the desired S/N ratio criterion. Obviously, we should select $\omega_o = \rho_s$ in an optimum design.

In the case when the laser beam from each diode is coherent, constructive interference[5] may occur, causing an optical beating signal in the detector. The upper limit of the crosstalk noise collected by a detector is given by

$$P_n = \{ 4[\frac{P_{n1}'}{4}]^{0.5} + 4[\frac{P_{n1}''}{4}]^{0.5} + 4[\frac{P_{n2}'}{4}]^{0.5} + 4[\frac{P_{n2}''}{4}]^{0.5} \}^2. \quad (9)$$

Such interference gives rise to the ghost spots at the detector plane[5]. For our purpose, the term coherent light sources means that the frequency separations between each laser diode is much smaller than the base bandwidth of the corresponding photodetectors. For investigating the free-space OI system shown in Fig. 1, Eqs. (4), (7), (8) and (9) are key formulae through which optimum system design can be obtained. They present the relationship among channel packing density, interconnection length and device design parameters.

To find the optimum design rules and system criteria, we define the S/N ratio as $N(dB) = 10 \times \log_{10} P_s/P_n$. In a high speed digital transmission system, the S/N ratio must be large enough to ensure the required bit-error-rate[13,14]. For example, 12 dB S/N is needed to ensure a bit-error-bit of 10^{-15} at a transmission rate of 500 MHz[13], which is equivalent to the clock speed of CRAY GaAs ECL machine.

3. Computer Simulations

Once the interconnect distance and the lens diameter are determined, the system performance is primarily determined by the ratio of detector diameter to lens diameter. Optimization of detector diameter in such an OI network is a pivotal factor. Fig. 5 shows the S/N ratio versus the detector-lens radius ratio with lens radius as a parameter (ω_o = 85, 100, 120 μm) based on Eqs. (4), (7), (8) and (9).

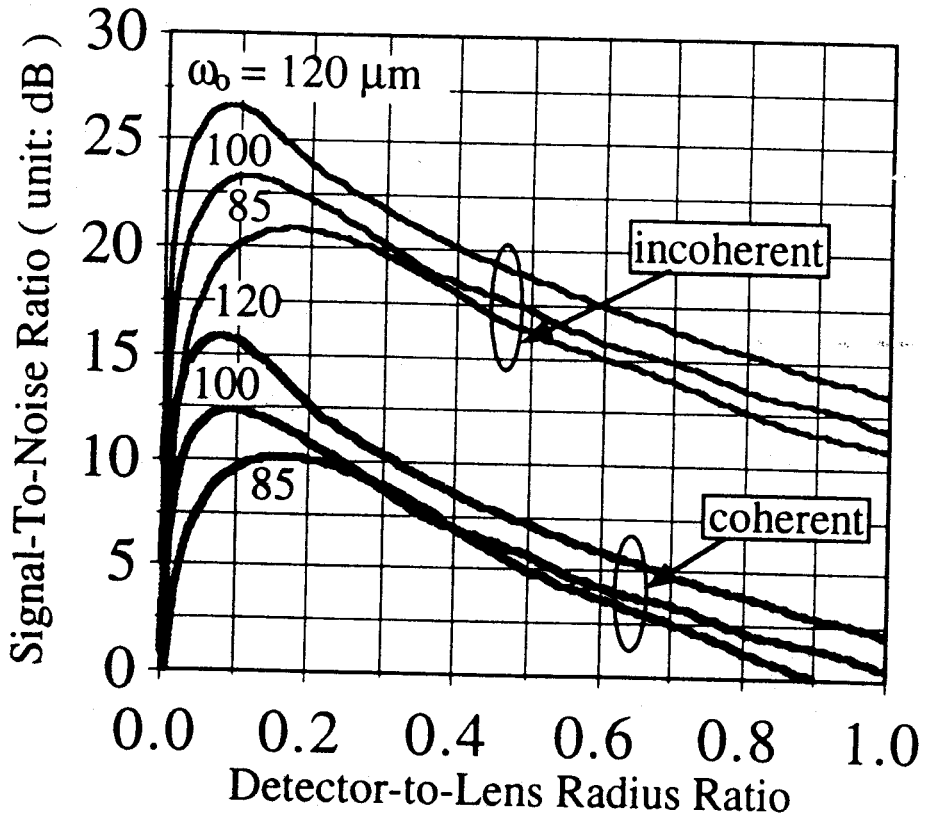

Figure 5: The signal-to-noise ratio versus detector-to-lens radius ratio with the lens radius as a parameter.

This figure indicates that the optimum photodetector radius ranges from 9 μm to 14 μm , corresponding to optical transmission efficiency from 35% to 60% based on Fig. 4. In order to increase the S/N ratio, it is the microlens aperture that needs to be enlarged rather than the photodetector size itself. In this simulation, a = 5 μm, λ = 0.85 μm, f = 500 μm and z = 5000 μm were assigned[5,6]. The S/N ratio is above 12 dB with the lens radius of 100 μm and detector radius of 9 μm (for coherent case). This is the standard size for both microlens and high speed (1 GHz/sec) photodetector, and corresponds to a channel packing density of 2500 pixels/cm^2 at an interconnection distance of 0.5 cm. Because of the high efficiency of the optical network based on both Fig. 4 and Fig. 5, no external laser driver, detector preamplifier, or other interface circuitry were required at a system clock of 1 GHz[2]. Fig. 5 also indicates that the coherent constructive interference from neighboring laser diodes may significantly reduce the S/N in highly parallel free-space optical interconnects.

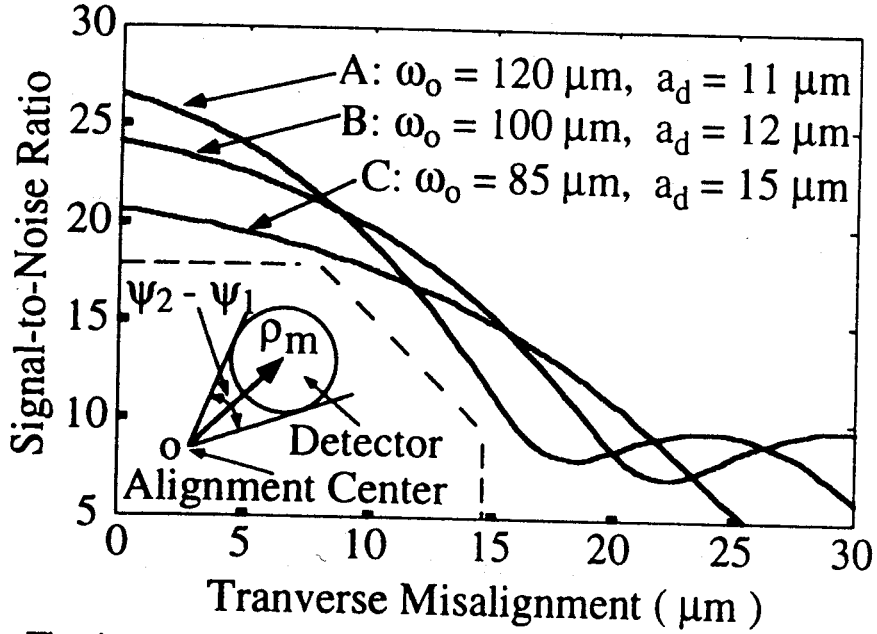

Figure 6: The signal-to-noise ratio versus transverse misalignment of photodetector array with the lens radius as a parameter.

The alignment of free-space optical interconnects is another important practical concern in system design. To evaluate the system sensitivity to misalignment, we further derive in Eq. (10) the variation of S/N as a function of the transverse misalignment (ρ_m) of the photodetector array, giving

$$S/N(\rho_m) = \frac{S_{\rho m}}{N_{\rho m}} = \frac{\int_{\rho_m}^{\rho_m + a_d} \int_{\psi_1}^{\psi_2} |E(\rho,\theta)|^2 d\rho d\theta}{P_{n1} + \int_{\rho_m}^{\rho_m + a_d} \int_{\psi_1}^{\psi_2} \sum_{n=1}^{4} |E_i(\rho,\theta)|^2 d\rho d\theta} , \qquad (10)$$

where P_{n1} is given by Eq. (4), $E(\rho,\theta)$ and $E_i(\rho,\theta)$ are derived from Eq. (6) and stand for, respectively, the diffraction fields from the detector's own lens and from the four nearest neighboring lenses, and ψ_2 -

ψ_1 (shown in the inset of Fig. 6) is the angle covered by the detector in reference to the alignment center in the detector plane. Fig. 6 shows the effect of transverse misalignment on S/N ratio for different detector radius and microlens radius combinations A, B, and C, based on Eq. (10). As indicated by Fig. 6, transverse misalignment is very critical in S/N reduction for all three different lens radii (ω_1 = 85 μm, ω_2 = 100 μm and ω_3 = 120 μm). The nonlinear variations of the S/N ratio shown in Fig. 6 are due to diffraction rings.

In order to study the sensitivity to longitudinal alignment, the relationship between S/N ratio and interconnect distance is plotted in Fig. 7 based on Eqs. (4), (7), (8) and (9). In Fig. 7, a = 5 μm, f = 500 μm, ω_o = 100 μm, and a_d = 12 μm were assumed. As shown in Fig. 7, the S/N ratio varies slowly around the designed interconnect distance of 0.5 cm, which indicates that the longitudinal alignment of the photodetector array is not as critical as the transverse alignment in the multi-stage optical interconnect network presented herein.

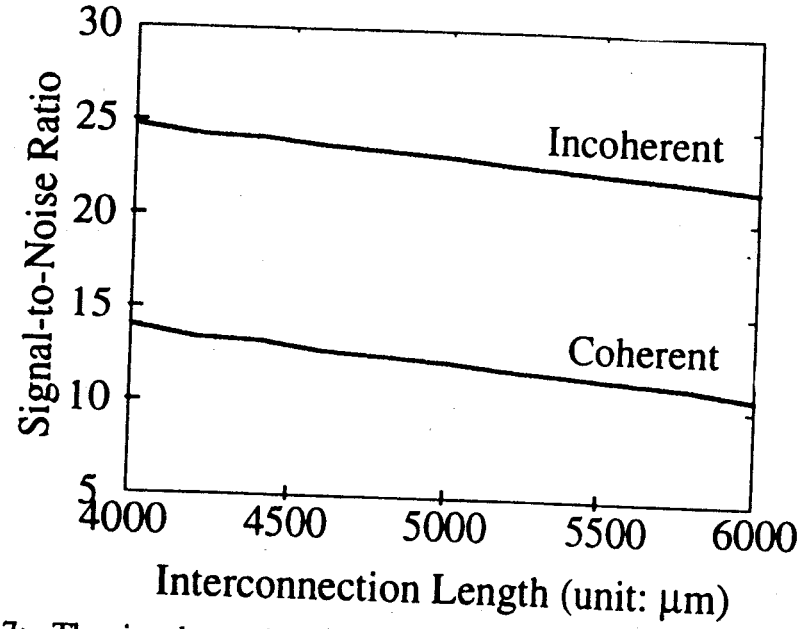

Figure 7: The signal-to-noise ratio versus optical interconnect length.

4. Experimental Results

In order to determine the accuracy of the formulas developed, the intensity distributions of laser beams through a linear microlens array were measured 0.5 cm away from the microlenses, which is equivalent to the interconnection distance presented in Fig. 2. Fig. 8 shows the measured spot profiles. In the experiment, the optical throughput of a VCSEL array was simulated by a HeNe laser (λ = 0.6328 μm) through a pinhole array with center-to-center separation of 200 μm and aperture of 10 μm[5]. The microlens array was positioned with the pinhole array at its focal plane so that the microlens array output beams were well collimated. The microlens employed has a radius of 85 μm and a focal length of 425 μm (see Fig. 1(b)). A 20x objective lens was used to enlarge the spot profile. The intensity distribution was measured by a Newport Optical Power Meter (Model 835) through a spatial filter. The pinhole array, microlens array and the 20x micro objective lens were mounted on three X-Y-Z translation stages,

respectively, with a resolution of ± 1 μm. In Fig. 8, the theoretical spot profiles based on Eq. (6) are also provided. The separation for adjacent pixels is 200 μm in Fig. 8.

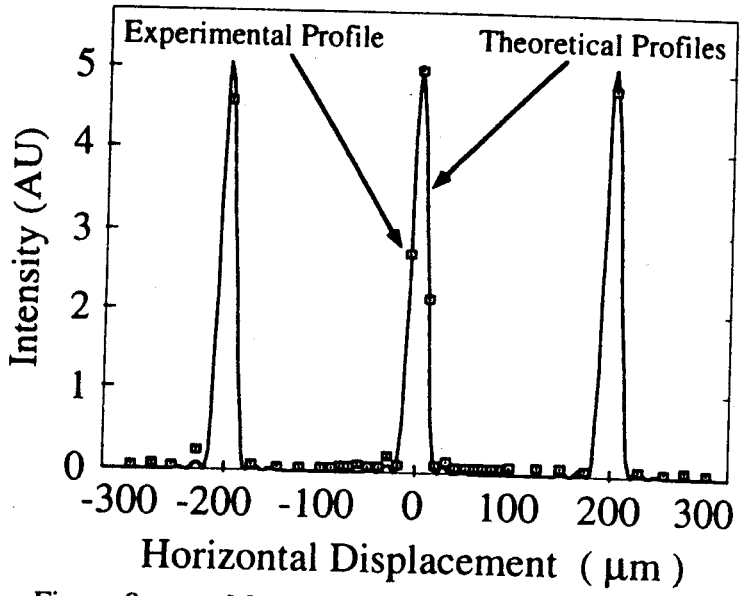

Figure 8: Measured and theoretical beam profiles.

Further experimental results are shown in Fig. 9. Fig. 9(a) is a photograph of the linear microlens array employed in the experiments, where f = 425 μm, ω_0 = 85μm, and lens-to-lens separation is 200 μm. Fig. 9(b) is a photograph of the propagating beam profiles obtained at the image plane z = 0.5 cm away from the microlens array, where a = 5 μm, λ = 0.6328 μm, and the pinhole-to-pinhole is 200 μm. In the experiment, the pinhole-to-lens separation was carefully adjusted to the focal length (f = 425 μm), so that the projecting beams were well-collimated. The beam profiles were then taken by a CCD camera.

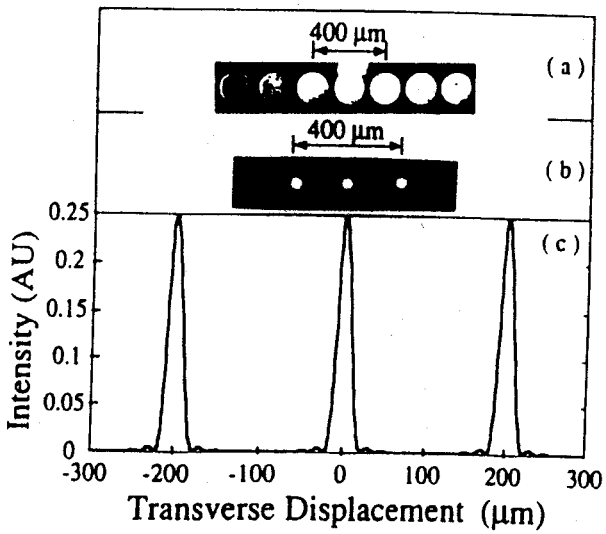

Figure 9: (a) Photograph of the microlens array employed, (b) Photograph of the propagating beams, and (c) Theoretical beam profiles using experimental parameters of Fig. 9(a) and 9(b).

Fig. 9(c) is the theoretical plot of the transverse intensity distribution of propagating beams based on Eq. (6), using experimental parameters of Fig. 9(a) and 9(b). As shown in Fig. 9, the agreement between the theoretical beam profiles (the full width at the first minimum and at the second minimum) and the experimental beam profiles is obvious. Good agreement was also found for an optical interconnect based on linear arrays of surface-emitting laser diodes and microlenses[6] by employing existing data and Eq. (6).

To further determine the transmission efficiency and system sensitivity to misalignment, an a_d = 15 μm spatial filter was placed at z = 0.5 cm away from the microlens on a X-Y-Z micro translation stage. The optical power transmitted through the spatial filter was detected as a function of the filter location in the plane perpendicular to laser beam. The measured power distribution is shown in Fig. 10. A nearly circular power distribution was obtained. In Fig. 10, 8% optical reflection loss of the microlens is added in the calculated profile from Eq. (10). As shown in Fig. 10, 25% (transmission efficiency) of the laser output (P_o) can be delivered to a photodetector at the plane of the receiver array. In order to increase the transmission efficiency, the radius of microlens employed should be enlarged. The optical power drops rapidly with the transverse misalignment of the spatial filter (photodetector). As shown in Fig. 10, the full width at half-maximum (FWHM) is 15 μm, which is about the size of pinhole aperture employed.

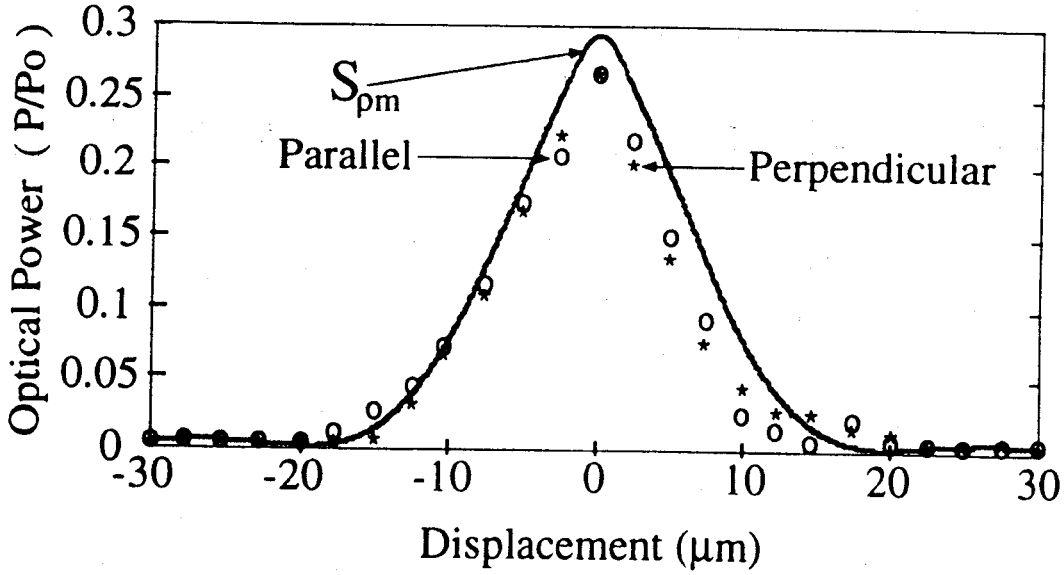

Figure 10: Optical power distribution contained in a pinhole with radius of 15 μm.

5. Concluding Remarks

Free-space optical interconnects based on arrays of VCSELs, microlenses, and photodetectors were analyzed based on the crosstalk model developed herein. The system performance and optimum design rules were investigated through computer aided analysis. Variations of packing density, interconnection distance and optical transmission efficiency were determined as design parameters for the arrays of VCSELs, microlenses and photodetectors. It was shown that it is pivotal to optimize the photodetector diameter in order to increase the system capabilities. The transverse alignment of the photodetector array is very critical compared with the longitudinal alignment. To verify the OI network and the theory presented herein, some experiments were conducted and the results showed good agreement with the theory presented. The feasibility of such a free-space OI network, with packing density of 2500 pixels/cm^2, interconnection distance of 0.5 cm, optical transmission efficiency better than 25%, and S/N